www.amlett.com, www.vbripress.com/aml, DOI: 10.5185/amlett.2015.5856 Published online by the VBRI Press in 2015

Structural, dielectric, magnetic and magnetoelectric characterization of $Co_{0.5}Ni_{0.5}Fe_2O_4$ - $Bi_{0.9}La_{0.1}FeO_3$ composite

Manjusha and K. L. Yadav*

Smart Materials Research Laboratory, Department of Physics, Indian Institute of Technology, Roorkee 247667, Roorkee, India

*Corresponding author. Tel: (+91) 1332 285744; Fax: (+ 91) 1332 273560; E-mail: klyadav35@yahoo.com

Received: 16 February 2015, Revised: 17 June 2015 and Accepted: 20 June 2015

ABSTRACT

Mixed spinel -perovskite composites of (x) $Co_{0.5}Ni_{0.5}Fe_2O_4$-(1−x) $Bi_{0.9}La_{0.1}FeO_3$(x = 0, 0.25, 0.40, 0.55, 1.0) have been synthesized by conventional solid state reaction method and annealed at 850 ºC. The X-ray diffraction (XRD) pattern shows that the composites consisted of spinel $Co_{0.5}Ni_{0.5}Fe_2O_4$ and rhombohedral perovskite $Bi_{0.9}La_{0.1}FeO_3$ ceramics. FESEM micrographs show closely packed microstructure with grain size in the range 503 nm - 960 nm. Variation of dielectric constant and dielectric loss with temperature at two fixed frequencies (500 kHz and 1 MHz) was studied. The composite with composition x = 0.55/sintered at 850 ºC exhibits the largest coercitivity (H_c) of 883 Oe. The saturation magnetization (M_s) and magnetic moment (μ_B) increase with an increase of $Co_{0.5}Ni_{0.5}Fe_2O_4$ concentration in the composites. From ferroelectric hysteresis loop analysis the values of remnant polarization (P_r) and coercive field (E_c) was found to lie in the range of 0.018-0.745 μC/cm^2 and 3.89-6.06 kV/cm. The relative change of magnetocapacitance was found to be 6.6% at a magnetic field of 8 kOe for x = 0.55 composition. Impedance analysis suggests the presence of a temperature dependent electrical relaxation in the material having a typical negative temperature coefficient of the resistance (NTCR) behavior analogous to a semiconductor.

Keywords: Composites; XRD; dielectric, ferroelectric; hysteresis loop.

Introduction

Multiferroic magnetoelectrics are materials that are both ferromagnetic and ferroelectric in the same phase [**1**]. The synthesis of materials that exhibits simultaneous ferromagnetic and ferroelectric characteristics has recently attracted a great deal of attention in research as well as in practical electronic devices [**2**]. Multiferroic magnetoelectric (ME) composite systems, such as ferromagnetic-ferroelectric heterostructures, which offer a novel route for integrating ferroelectric and ferromagnetism, have been widely studied in recent years [**3**]. From the view point of material constituents, multiferroics ME materials can be divided into two types: single phase and composite. The single-phase multiferroics exhibit the coexisting order parameters only at low temperatures, and they additionally have weak magnetoelectric response at room temperature. To overcome the problems of single-phase multiferroics, magnetoelectric composites have been developed, and it has been found that a much stronger ME coupling effect is expected to be realized in a composite of piezoelectric phase and magnetostrictive phase by using product properties [**4**]. Magnetoelectric coupling describes the influence of a magnetic (electric) field on the polarization (magnetization) of a material. It may arise directly between the two order parameters as in ME composites. ME effect in composites is due to induced strain in the piezomagnetic phase by the application of magnetic field that is mechanically coupled to induce stress in the piezoelectric phase that results into the generation of induced voltage.

In the past years, various magnetoelectric composites have been developed such as $CoFe_2O_4$-$BiFeO_3$ [**5**], $BiFeO_3$-$NiFe_2O_4$ [**6**], $Ni_{0.75}Zn_{0.25}Fe_2O_4$-$BiFeO_3$ [**7**], $CrFe_2O_4$-$BiFeO_3$ [**8**], $MnFe_2O_4$-$BiFeO_3$ [**9**], $BiFeO_3$-$BaTiO_3$ [**10**], $Ni_{0.8}Zn_{0.2}Fe_2O_4$-$Ba_{0.6}Sr_{0.4}TiO_3$ [**11**], $BiFe_{0.5}Cr_{0.5}FeO_3$-$NiFe_2O_4$ [**12**], $BiFeO_3$-$CoFe_2O_4$ nanostructures [**13**] and multiferroic $BiFeO_3$-$CoFe_2O_4$ nanocomposites [**14**]. Besides this several efforts have been made by making composite film of CFO-BFO [**15-16**]. A suitable combination of ferrite and ferroelectric materials is very significant to get better ME effect. For this, the magnetostriction coefficient of ferrite phase and piezoelectric coefficient of ferroelectric phase must be high [**17, 18**]. BFO-based single phase multiferroics generally have weak macroscopic magnetic properties which lead to weak magnetoelectric (ME) effect in these materials. La doping in BFO reduce the leakage current and also to release the potential magnetization locked in the spiral spin structure [**19**]. The substitution of Bi^{3+} by La^{3+} is favorable

for stabilizing the perovskite phase due to the similar radii values of Bi^{3+} (1.030 Å) and La^{3+} (1.032 Å), and La doping at the Bi site enhances the ferromagnetic property of BFO [**20**]. La doping in BFO (at A site) helps to improve the electrical and magnetic properties by suppressing the growth of secondary phases [**21**].

Spinel $CoFe_2O_4$ is a well-known hard magnetic material, which has been studied in detail due to its high coercivity (5400 Oe) and moderate saturation magnetization (about 80 emu/gm) as well as its remarkable chemical stability and mechanical hardness [**22**]. Nickel doped cobalt ferrite exhibits a semiconducting nature up to 513 K for all the compositions and underwent to metallic phase above 513 K. It is attributed to cation distribution between A and B sites as a function of temperature [**23**]. Moreover Co–Ni ferrites has the high electrical resistivity and a good magnetic property which is suitable for high-frequency electronic device applications in the telecommunication field [**24**]. Keeping in view these aforesaid facts, this paper presents a systematic study of structural, dielectric, magnetic, magnetodielectric and ferroelectric properties of (x) $Co_{0.5}Ni_{0.5}Fe_2O_4$-(1–x) $Bi_{0.9}La_{0.1}FeO_3$ (x = 0, 0.25, 0.40, 0.55, 1.0) composite prepared by hybrid processing route containing $Co_{0.5}Ni_{0.5}Fe_2O_4$ (CNFO) as ferrite component and $Bi_{0.9}La_{0.1}FeO_3$ (BLFO) as ferroelectric component.

Experimental

The Composite of (x) $Co_{0.5}Ni_{0.5}Fe_2O_4$-(1−x) $Bi_{0.9}La_{0.1}FeO_3$ having two different phases were prepared by a conventional solid state reaction method. For ferrite phase stoichiometric amounts of Co_3O_4, NiO and Fe_2O_3 were mixed in an acetone media for 5-6 h. Then mixed powder was dried and the resultant mixture was then calcined at 1100 ºC for 6 h in air atmosphere and for ferroelectric phase taking amounts of $Bi(NO_3)_3.5H_2O$, $La(NO_3)_3.6H_2O$ and $Fe(NO_3)_3.9H_2O$ in stoichoimetric propotion. Initially, Bi $(NO_3)_3.5H_2O$ were dissolved into 150 ml distilled water with few drops of Nitric acid. Then this solution was heated on a hot plate under constant stirring with magnetic stirrer until the solution becomes transparent. In another beaker we put 30 ml water and 7 ml ethyelene glycol and 4 gm citric acid and then mix it with that previous transparent solution and then add $La(NO_3)_3.6H_2O$ and $Fe(NO_3)_3.9H_2O$. This mixture kept for 2 h on a hot plate under constant stirring until the solution converted to gel, then these precursor solution was dried at 70 ºC in an oven overnight then the dried gel was mixed in an agate mortar. Ground precursor powders were calcined in air for 2 h at 600 ºC. The calcined powder was then leached in diluted HNO_3 to eliminate the impurity phase from BLFO. The powders of both ferrite and ferroelectric phase obtained after calcination were mixed for 5-6 h to get the desired composite. The ferroelectric–ferrite composites (x) $Co_{0.5}Ni_{0.5}Fe_2O_4$-(1−x) $Bi_{0.9}La_{0.1}FeO_3$ where x = 0, 0.25, 0.40, 0.55 and 1.0 were prepared by mixing CNFO and BLFO according to the above mentioned formula. After this, these mixtures were then pressed into the form of pellets of 9 mm diameter and 1.5 mm thickness with a pressure of about 7.56 × 10^7 kg/m^2. The structure of the samples was determined by X-Ray diffractometer with Cu (Kα) (λ=1.5402 Å) radiation, at Bragg angle (20º ≤ 2 θ ≤ 60º) with a scanning speed of 1º min^{-1} at room temperature. The dielectric measurements were done by using a LCR Meter in the temperature range 35-450 ºC (500 kHz and 1 MHz) was used to measure dielectric properties. Microstructure analysis was carried out by FESEM. Magnetodielectric measurement was carried out using a magnet up to 8,000 Oe. The magnetic properties of composites were analysed by using a Vibrating Sample Magnetometer (VSM) with magnetic field in the range of (−10,000 Oe ≤ H ≤ 10,000 Oe). The hysteresis curve was carried out using a modified Sawyer–Tower circuit.

Results and discussion

Structural analysis

The XRD patterns of composites of (x) $Co_{0.5}Ni_{0.5}Fe_2O_4$-(1−x) $Bi_{0.9}La_{0.1}FeO_3$ where x = 0.25, 0.40, 0.55 with the individual phases of CNFO and BLFO are shown in **Fig. 1**.

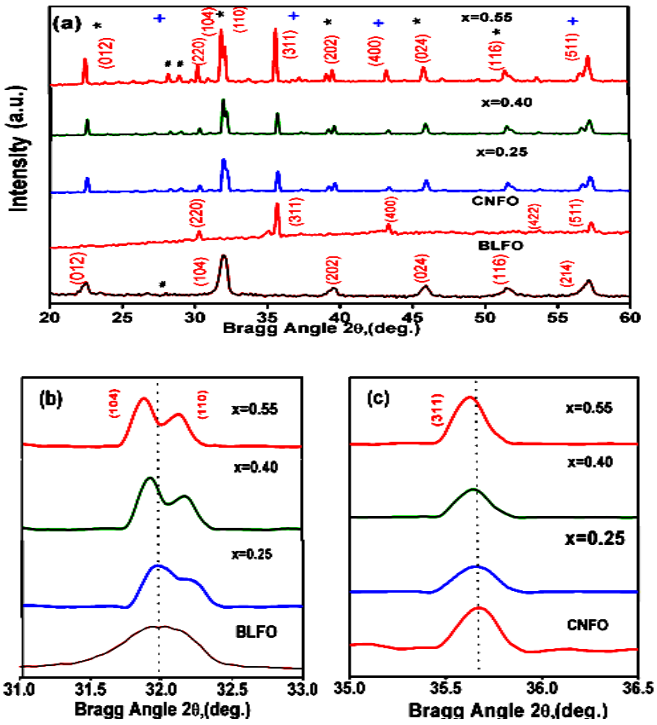

Fig. 1. (a) X-ray diffraction patterns for (x) CNFO - (1−x) BLFO where x = 0.25, 0.40, 0.55 composites with (CNFO) and (BLFO), where (⋆) denote the BLFO phase and (+) denote the CNFO phase (b) Showing the shifting of BLFO (104) peak and (c) shifting of CNFO (311) peak in composites for (x = 0.25, 0.40, 0.55) and (# marked $Bi_2Fe_4O_9$ impurity phase).

Few low intensity peaks are also observed in the BLFO ceramic in the range (2θ~ 27º- 29º). These peaks show the presence of bismuth ferrite impurity phase of $Bi_2Fe_4O_9$ (# marked) in the BLFO ceramics. The XRD pattern of all the three compositions shows mixed crystalline spinel-perovskite phases. The ferrite phase CNFO has cubic spinel structure having lattice parameter a = 8.338 Å and ferroelectric phase BLFO has orthorhombic phase, which can also be described by hexagonal system of basis with lattice parameter a_{hex} =5.615 Å and c_{hex} =13.542 Å corresponding to c/a ratio of 2.411. It can be observed that with the incorporation of CNFO, the most intense peaks

(104) of BLFO splits into two peaks (104) and (110). This indicates a change in structure of the ferroelectric phase as shown in **Fig. 1(b)**. This means there is structural transformation from orthorhombic to rhombohedral phase. The major peak of CNFO (311) shifted to lower angles as shown in **Fig. 1(c)** indicating distortion of the CNFO lattice. The values of lattice parameters calculated for the individual phases in the composites with x = 0, 0.25, 0.40, 0.55, and 1.0 are shown in **Table 1**. This is also confirmed from the fact that the c/a ratio in our CNFO-BLFO composites (as shown in **Table 1**) is larger than that of pure BLFO ceramic, this suggests the diffusion of Co^{2+} or Ni^{2+} into the BLFO lattice from the CNFO phase [**25**]. The ionic radii of Co^{2+} (0.78 Å) and Ni^{2+} (0.69 Å) are larger than the ionic radius of Fe^{3+} (0.64 Å)**.** Substitution of Co^{2+} (0.78 Å) or Ni^{2+} (0.69 Å) at the Fe^{3+} (0.64 Å) site of BLFO can result increase of the BLFO parameters because of its larger radius than Fe^{3+} (0.64 Å) [**26**]. Therefore, the observed increase in the lattice parameters of the CNFO-BLFO composite in comparison to the BLFO ceramic may be attributed to the diffusion of Fe^{3+} into the BLFO lattice during sintering process.

Microstructural study

FESEM micrographs of (x) $Co_{0.5}Ni_{0.5}Fe_2O_4$ - (1−x) $Bi_{0.9}La_{0.1}FeO_3$ composites where x = 0, 0.25, 0.40, 0.55 and 1.0 are shown in **Fig. 2(a)-(e)**, consisting of randomly oriented, non-uniform (both in shape and size) closely packed grain in the composites. The mixed microstructures of the composites with different grain size and few pores are clearly revealed from the micrographs. The average grain size (**Table 1**) of the composites calculated using ASTM E112-13 are found to be 503, 747, 960, 831, and 887 nm for (x) $Co_{0.5}Ni_{0.5}Fe_2O_4$ - (1−x) $Bi_{0.9}La_{0.1}FeO_3$ where x = 0, 0.25, 0.40, 0.55 and 1.0.

Table 1. Lattice parameters of (x) $Co_{0.5}Ni_{0.5}Fe_2O_4$ - (1−x) $Bi_{0.9}La_{0.1}FeO_3$ composites with (a) x = 0, (b) x = 0.25, (c) x = 0.40, (d) x = 0.55, (e) x = 1.0.

Composition (x)	Lattice parameters of phase			c/a	Grain Size (nm) {ASTM E112-13}
	Ferrite	Ferroelectric			
	a (Å)	a (Å)	c (Å)		
0	----	5.615	13.542	2.411	503
0.25	8.330	5.592	13.500	2.414	747
0.40	8.333	5.596	13.521	2.416	960
0.55	8.338	5.612	13.593	2.422	831
1.0	8.343	----	----	----	887

The average grain size of the composites is found to increase with CNFO addition. This increase of grain size resulted into reduction of porosity which leads to the densification of ceramic composites with increasing ferrite content. The compositional analysis for (x) $Co_{0.5}Ni_{0.5}Fe_2O_4$ - (1−x) $Bi_{0.9}La_{0.1}FeO_3$ with x = 0.40, determined by EDX analysis is shown in **Fig. 2(f)**. The purity and confirmation of formation of composites is revealed from the presence of expected elements (Co, Ni, Fe, Bi, La, and O) in the EDX spectra. **Fig. 3** shows elemental mapping in the composite of 0.55CNFO-0.45BLFO. It shows uniform distribution of Fe, O, Bi, Co, Ni and La in the synthesized composite.

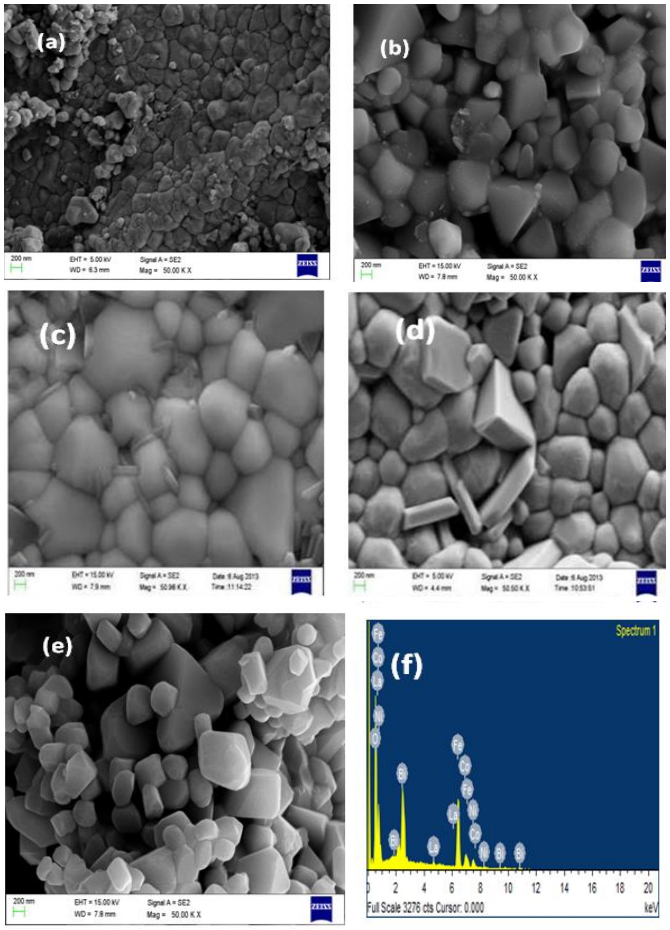

Fig. 2. FESEM micrographs of (x) $Co_{0.5}Ni_{0.5}Fe_2O_4$ - (1−x) $Bi_{0.9}La_{0.1}FeO_3$ composites with (a) x = 0, (b) x = 0.25, (c) x = 0.40, (d) x = 0.55, (e) x = 1.0 and (f) EDX spectrum of composite with x = 0.40.

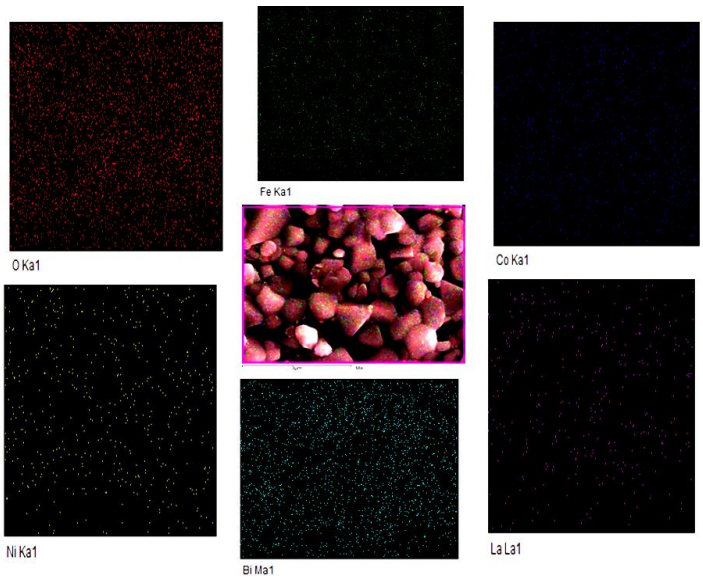

Fig. 3. Elemental mapping showing distribution of different elements in 0.55 $Co_{0.5}Ni_{0.5}Fe_2O_4$ – 0.45 $Bi_{0.9}La_{0.1}FeO_3$ composites.

Dielectric constant and dielectric loss variation with temperature

The variation of dielectric constant and dielectric loss with temperature for (x) CNFO- (1-x) BLFO (where x = 0, 0.25,

0.40, 0.55 and 1.0) ceramics measured at two different frequencies (500 kHz and 1 MHz) are shown in **Fig. 4(a)-(e)** and the variation of dielectric constant and dielectric loss with CNFO concentration at room temperature and 1 MHz are shown in **Fig. 4(f)**. This dielectric constant versus temperature curve shows a broad peak around 360 °C, this dielectric anamoly is attributed to the antiferromagnetic transition of the sample, as we know that $BiFeO_3$ has an antiferromagnetic transition (T_N) at 370 °C.

The anamoly in the dielectric constant may be due to the magnetoelectric coupling effects which are predicted by Landau- Devonshire theory of phase transition in magnetoelectrically ordered systems [**27**]. In this context, we observed the dielectric peaks near around the antiferromagnetic Neel temperature (T_N ~ 370 °C) of $BiFeO_3$. The antiferromagnetic transition temperature decreased with increasing concentration of CNFO.

The small value of dielectric constant of BLFO ceramics may be due to the oxygen vacancies and the displacement of Fe^{3+} ions. The value of dielectric constant is got enhanced with increasing CNFO content may be due to the conduction mechanism caused by hopping of electrons between Fe^{2+}/Fe^{3+}, Co^{2+}/Co^{3+}, and Ni^{2+}/Ni^{3+} ions which are responsible for conduction mechanism. Moreover the peaks of dielectric constant shift to high temperature with increasing frequency [**28**]. This is due to the relaxor behavior of the composites. From **Fig. 4(f)** we see that the dielectric constant is increasing with the increasing ferrite content. In addition, the formation of barrier layers at the grain and grain boundary interfaces give rise to interfacial space charge polarization. This kind of behaviour exhibiting high dielectric constant at low frequency and the low value at high frequency is a mark of large Maxwell-Wagner type dielectric dispersion [**29**]. The composite with x = 0 and 1.0 exhibits diffuse phase transition (DPT) with broad maxima in the dielectric behaviour and the maxima shifts to higher temperature side with increase of frequency. The cation disorder due to nanoscaled ordered microregions in complex perovskite is generally responsible for DPT [**30**]. Moreover this diffuse phase transition observed in composites is ascribed to the fact that the ferroelectric grains are interconnected to non-ferroelectric grains, as reported earlier for composites [**31**]. The increase of dielectric constant with addition of CNFO content can also be ascribed to increase of average grain size with CNFO content (**Table 1**). The increase of average grain size leads to reduction of grain boundary area which acts as an obstacle for domain wall motion. The mean free path of electrons increases with increases of grain size and hence the dielectric constant [**32**]. At higher temperatures there is rapid increase of dielectric loss which indicates the increased space charge conduction which is further related to the movement of oxygen vacancies towards dielectric-electrode interface [**30**]. The Dielectric loss is found to increase with CNFO concentration this is due to the conduction mechanism in ferrites. On the basis of Verwey de Bohr mechanism, the conduction phenomenon in ferrites is explained which involves the exchange of electrons between ions of same elements existing in more than one valence state and are randomly distributed over equivalent crystallographic lattice sites [**7**].

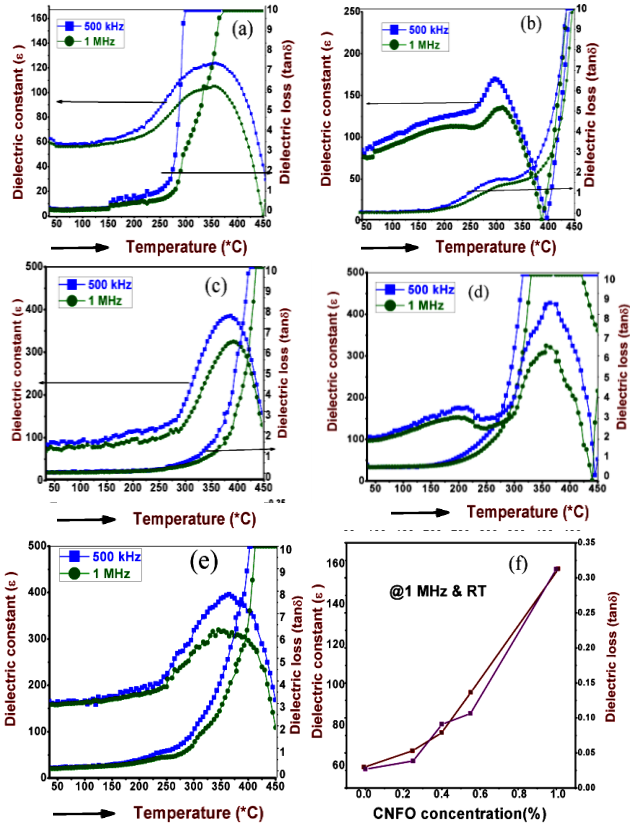

Fig. 4. (a)-(e) Dielectric constant with temperature for (x) CNFO- (1-x) BLFO where x = 0, 0.25, 0.40, 0.55, and 1.00 and (f) Variation of dielectric constant and dielectric loss with different CNFO concentration.

Magnetic measurement

The magnetic properties of the (x) CNFO- (1-x) BLFO (with x = 0, 0.25, 0.40, 0.55 and 1.0) using a VSM with an applied field of -10,000 Oe ≤ H ≤ 10,000 Oe are analysed at room temperature are shown in **Fig. 5 (a)**. The value of saturation magnetization ($2M_s$) and remnant magnetization ($2M_r$) with the CNFO content shown in **Fig. 5(b)**. M-H hysteresis loop at room temperature shows that there is the presence of an ordered magnetic structure [**28**] as due to the presence of CNFO the spin cycloid of BLFO is suppressed and locked magnetization is released. The magnetic moment in Bohr magneton has also been calculated using the following relation (1):

$$\mu_B = \frac{M\sigma's}{5585} \quad (1)$$

where, M is the molecular weight, σ_s' is the magnetization per gram mol of the sample and 5585 is the magnetic factor. The value of saturation magnetization (M_s) (shown in **Fig. 5(b)**) increases with the increasing amount of ferrite content due to the fact that the individual ferrite grains act as centers of magnetization. All the measured magnetic parameters are listed in the **Table 2**.

An enhancement in the remanence (Mr) and saturation magnetization is observed with increasing CNFO concentration. The value of Ms in our composite is comparable with those of the BFO-CFO composite [**5**].

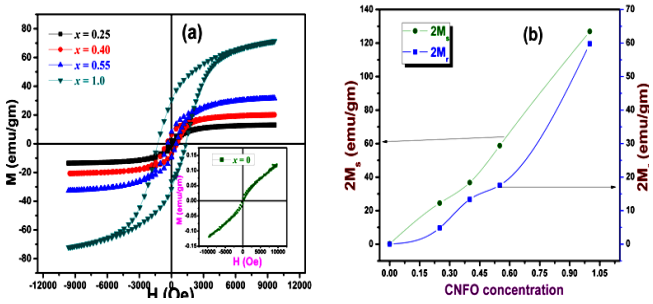

Fig. 5. (a) Room temperature M-H loops of (*x*) CNFO - (1-*x*) BLFO where *x* = (0, 0.25, 0.40, 0.55 and 1.0) composites, (b) Saturation magnetization (M_s) and Remnant magnetization (M_r) with different CNFO content.

Table 2. Data on magnetic parameters of (*x*) $Co_{0.5}$ $Ni_{0.5}Fe_2O_4$ - (1-*x*) $Bi_{0.9}La_{0.1}FeO_3$ composites with *x* = 0, 0.25, 0.40, 0.55, 1.0.

Composition	Remnant Magnetization ($2M_r$) emu/gm	Saturation Magnetization ($2M_s$) emu/gm	Coercivity ($2H_c$) kOe	Magnetic Moment (μ_B)
x = 0	0.0167	0.183	0.429	0.010
x = 0.25	4.842	24.499	0.474	1.263
x = 0.40	13.366	36.752	0.942	1.824
x = 0.55	17.564	58.766	0.786	2.805
x = 1.00	59.81	126.94	2.635	5.329

The increase in the value of saturation magnetization and coercitivity with an increasing CNFO content due to the substitution of Co^{2+} or Ni^{2+} into the BLFO ceramics at the B site (Fe^{3+} site). The sample with *x* = 0.55 exhibits coercivity, $2H_c$ of 786 Oe and the higher saturation magnetization ($2M_s$) of 58.766 emu/gm, obtained by extrapolated value at 10 kOe. The magnetism observed in our composites can be due to the combined effects of BLFO and CNFO. The contribution of magnetization in our composites is mainly due to the CNFO, which has higher value of magnetization as compared to BLFO. The observed magnetization due to the change in bond angle of Fe-O-Fe caused by the distortion created by substitution of Bi or La by Co or Ni may allow the canting of the antiferromagnetic sublattices. Moreover this substitution is able to break the cycloidal structure of BLFO matrix, and it will release the macroscopic magnetization [**33**]. A ferromagnetic material is said to have magnetocrystalline anisotropy if it takes more energy to magnetize it in certain directions than in others. The spin-orbit interaction is the primary source of magnetocrystalline anisotropy. Bulk $CoFe_2O_4$ is characterized by a strong cubic anisotropy of magnetocrystalline origin, mainly due to the Co^{2+} ions, which have non zero orbital momentum [**34**]. In a single-domain particle with volume V and effective magnetic anisotropy K_{eff}, the reversion of the magnetic moment over the anisotropy energy barrier $E_a = K_{eff}$ V is assisted by thermal phonons [**35**]. The main contribution of electrical conductivity at high temperatures generally originates from thermally activated oxygen vacancies. The temperature dependence conductivity follows the Arrhenius equation $\sigma = \sigma_0 \exp(-E_a / k_B T)$, where σ_0 is the pre-exponential factor, Eα is the activation energy per charge carrier, k_B is the Boltzmann's constant and T (K) is the absolute temperature [**36**]. From **Fig. 6 (a)**, we have calculated the activation energy E_a = 0.7048 eV by the slop of this curve in which data is taken after the transition temperature (T_c) and volume of CNFO lattice is 580.71 $Å^3$ and by using this formula $E_a = K_{eff}$ V we have found that K_{eff} is 19.44×10^8 ergs/cm^3.

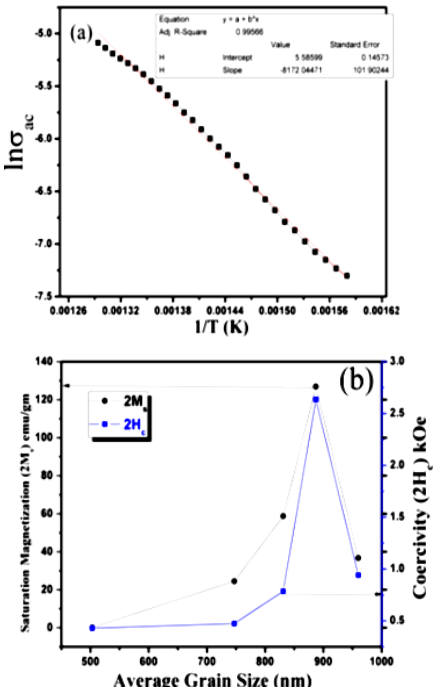

Fig. 6. (a) Variation of ac conductivity of $Co_{0.5}$ $Ni_{0.5}Fe_2O_4$ to calculate the activation energy, (b) Variation of Coercivity and saturation magnetization with different average grain size in composites.

The variation of coercivity and saturation magnetization with grain size is shown in **Fig. 6 (b)**. We observed that at first the coercivity increases with increasing in grain size and reaches maximum for grain size 747 nm and afterwards it decreases, because when the particle size increases, the coercivity of the "single-domain" particle assembly increases, since the magnetic moment of the individual particle increases, and the magnetic anisotropy energy increases and therefore stronger field is required for magnetization reversal. Coercivity decreases for larger grain sizes has due to the crossover from single domain to multidomain behavior with increasing size [**37**].

In the single domain region, the coercivity varies according to the formula **[38]** Hc = (g-h/$D^{3/2}$), where g and h are constants and Hc is coercivity and D is particle size. Therefore, H_c increases as D increases below a critical particle size. However in multidomain region the coercivity varies according to the formula: Hc = (a + b/D), where a and b are constant and Hc is coercivity and D is particle size. Therefore coercivity decreases with the increasing particle size [**39**]. In our composites the particle with x =0, 0.25, and 0.40 having grain sizes 503 nm, 831 nm, and 960 nm respectively behaves as a multidomain because they have small coercivity having larger grain sizes and the particle with x =0.55, and 1.0 behaves as single domain particle because they have higher coercivity with their increasing grain sizes. Moreover smaller grains have a lower probability for strong surface defects and hence they achieve higher coercivities [**40**] and particles with multidomains require fewer magnetic fields to switch compared with the single domain state. From **Fig. 6(b**) we

observe that the value of saturation magnetization first increases with grain size and reaches maximum for grain size 887 nm and afterwards it decreases having grain size 960 nm (x = 0.40) because it behaves like a multidomain and for multidomain the variation saturation magnetization with particle size is given by Ms = $\sqrt{\frac{9\sigma_{\omega}}{2\pi D_m}}$, where D_m is the critical particle size and σ_{ω} is domain wall energy so M_s decreases with increasing particle size [**40**].

Magnetodielectric measurement

Fig. 7 shows the variation of magnetocapacitance with the magnetic field from 0 to 8,000 Oe and the measuring frequency is 1000 Hz. The Magnetocapacitance is defined as follows (2):

$$MC = \frac{\varepsilon(H) - \varepsilon(0)}{\varepsilon(0)} \times 100 \qquad (2)$$

where, ε (H) and ε (0) is the dielectric constant in the presence and absence of magnetic field respectively. The absolute value of magnetocapacitance increases with ferrite concentration in the composite. The change in the dielectric constant under the variation of magnetic field can be induced by magnetostriction effect, which occurs due to the change in lattice parameters on applying magnetic field [**41**]. If we apply magnetic field to a magnetoelectric material, the material gets strained, and this strain further induces stress which gives rise to an electric field. This generated field is able to orient the ferroelectric domains, and hence dielectric behavior is changed [**42**]. Since we have seen that due to barrier layer formation grain boundaries are more resistive than grains, so that the most of the field is dropped across the layers, and thus the apparent decrease in dielectric thickness results in an increased capacitance [**43**].

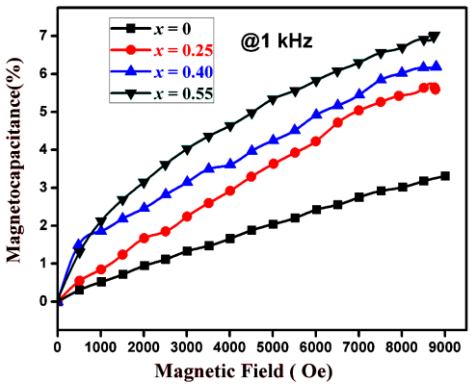

Fig. 7. The graph demonstrates the variation of magnetocapacitance with magnetic field for (*x*) $Co_{0.5}Ni_{0.5}Fe_2O_4$- (1−*x*) $Bi_{0.9}La_{0.1}FeO_3$ where *x* = 0, 0.25, 0.40, 0.55 and 1.0 composites at room temperature.

The magnetocapacitance in the system could also be attributed to the presence of magnetostriction or magnetoresistance effect. The magnetoresistance was also calculated for the samples, and it has been found that there is negligible variation of magnetoresistance with an applied magnetic field. This means that the magnetocapacitance in the system is not due to the magnetoresistance. The negative or positive sign of magnetodielectric effect depends on the product of spin-pair correlation of neighboring spins and the coupling constant [**44**]. The value of magnetocapacitance is found to increase with increase in the concentration of CNFO. The values of MC for (*x*) $Co_{0.5}Ni_{0.5}Fe_2O_4$ - (1− *x*) $Bi_{0.9}La_{0.1}FeO_3$ with *x* = 0, 0.25, 0.40 and 0.55 are found to be 2.8, 5.1, 5.8 and 6.6 %, respectively. The value of magnetocapacitance in our composites is found to be higher as compared to earlier reported composites as shown in **Table 3**.

Table 3. Values of magnetocapacitance (%) in the composites of CNFO and BLFO @1kHz and 8 kOe.

Materials	*x*	MC %	Reference
(1−*x*) $BaTiO_3$ - *x* $CoFe_2O_4$	0.43	1.8	[45]
$CoFe_2O_4$–$BaTiO_3$ nanostructures on Nb-doped $SrTiO_3$	---	2.0	[46]
(1−*x*) (0.3$CoFe_2O_4$-0.7$BiFeO_3$)-*x* $BaTiO_3$	0.40	3.4	[28]
x $NiFe_2O_4$ - (1−*x*) $BiFeO_3$	0.40	4.7	[6]
x $Co_{0.5}Ni_{0.5}Fe_2O_4$ - (1−*x*) $Bi_{0.9}La_{0.1}FeO_3$	0.40	5.8	Our result

Ferroelectric behaviour

Fig. 8(a)-(e) shows the room temperature ferroelectric hysteresis (P-E) measurements for the pure BLFO along with CNFO-BLFO composites which shows the ferroelectric behaviour of the composites.

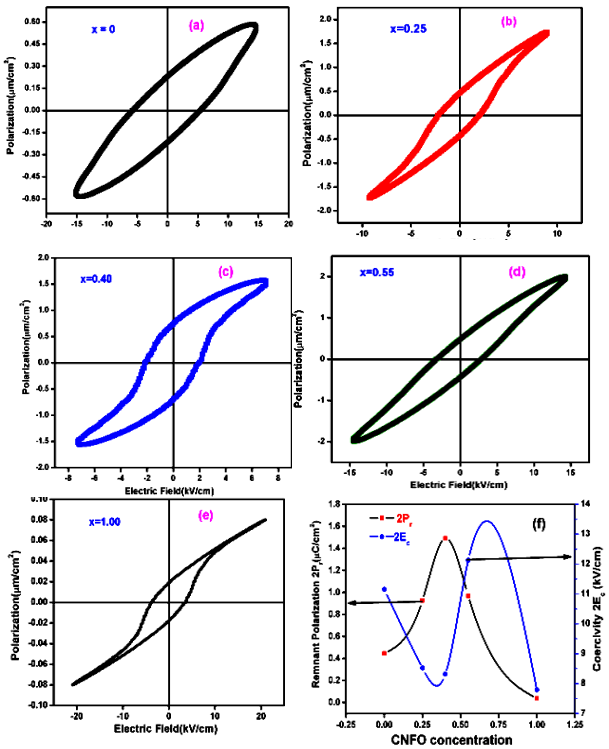

Fig. 8. P-E Hysteresis loops of (*x*) $Co_{0.5}Ni_{0.5}Fe_2O_4$ - (1− *x*) $Bi_{0.9}La_{0.1}FeO_3$ (a) *x* = 0, (b) *x* = 0.25, (c) *x* = 0.40, (d), *x* = 0.55 and (e) *x* = 1.0, composites at room temperature & (f) variation of remnant polarization, and coercivity of (*x*) $Co_{0.5}$ $Ni_{0.5}Fe_2O_4$ - (1−*x*) $Bi_{0.9}La_{0.1}FeO_3$ composites.

It is a most important character to study the ferroelectric behavior. From **Fig. 8**, it is revealed that all the samples except x = 0 have clear hysteresis loop, but as the CNFO contents increases, the P-E loops becomes narrow, which indicates that the ferroelectric order of BLFO is disrupted by the addition of CNFO. The variation of remnant polarization ($2P_r$) and coercive field ($2E_c$) with CNFO content are shown in **Fig. 8 (f)**. The high coercive field and leakage current may be responsible causes for unsaturated PE loop and low value of polarization in BFO [**47**]. However in case of smaller grains, the movement of domain wall is restricted through the grain boundary [**48**]. Moreover due to much lower resistance of the ferrite phase the composite ceramics are not fully polarised. The polarization of ferrites having lower resistance becomes difficult as they can withstand only low voltages [**49**]. The saturation has not been achieved in PE loops as they are dominated by leakage current originated from valence of Fe ions. The larger leakage currents in magnetoelectrics often result from mixed valence for the magnetic ions (e.g., Fe^{2+} and Fe^{3+}), from oxygen vacancies, or from both. The electrical hysteresis requires metal contacts and permits charge injection and real current flow [**50**]. Hence the obtained PE loop in **Fig. 8(a)** is not due to the polarization displacement current j = dP/dt but due to the conduction current j = σE.

Impedance analysis

The temperature dependence of complex impedance plots (Z*) or cole–cole plots i.e. plotting imaginary part Z″ against the real part Z′ of complex impedance Z*= Z′− jZ″ of (x) $Co_{0.5}Ni_{0.5}Fe_2O_4$ - (1−x) $Bi_{0.9}La_{0.1}FeO_3$ where x = 0, 0.25, 0.40, 0.55 and 1.0 composites performed at 250 ºC, 300 ºC, 350 ºC, 400 ºC, 450 ºC and 500 ºC over a wide frequency range (100 Hz–1 MHz) are shown in **Fig. 9**. The complex impedance plots of x = 0 sample (which has small and uniform average grain size) shows the large semicircle and the samples with CNFO concentration show quite small semicircles due to their gaint grain sizes. According to the Koops' model ferrite is a grain structured conductor in which layers of poorly conducting grain boundary material separates the grains [**51**]. We do not get semicircles above 300 ºC due to the high conductivity of BLFO, but in **Fig. 9(b-e)** with increasing temperature the semicircles make larger intercepts on the real X-axis indicating increase in the impedance of the sample on CNFO doping. It is observed that all the semicircles arc exhibits some degree of depression indicating that centres of these semicircles lies below the real Z′ axis, showing presence of non-Debye type of relaxation in the material.

The non-Debye type nature of dielectric relaxation could be analysed through complex impedance plots. Impedance spectra shows the formation of semicircular arc for the high temperature (250-500 °C), which depends upon the strength of the relaxation and available frequency range for the experiments. The impedance spectra are characterized by the appearance of two semicircles, larger radii and a small radii corresponding to the high and low frequency region, indicating the effects of bulk and grain boundary effects respectively, whose radii of curvature decreases with an increase in temperature such that their centre lie below the real axis. Semicircles are observed below 350 °C and above this temperature the grain boundary resistances cannot be separated out, as there are no complete semi circles.

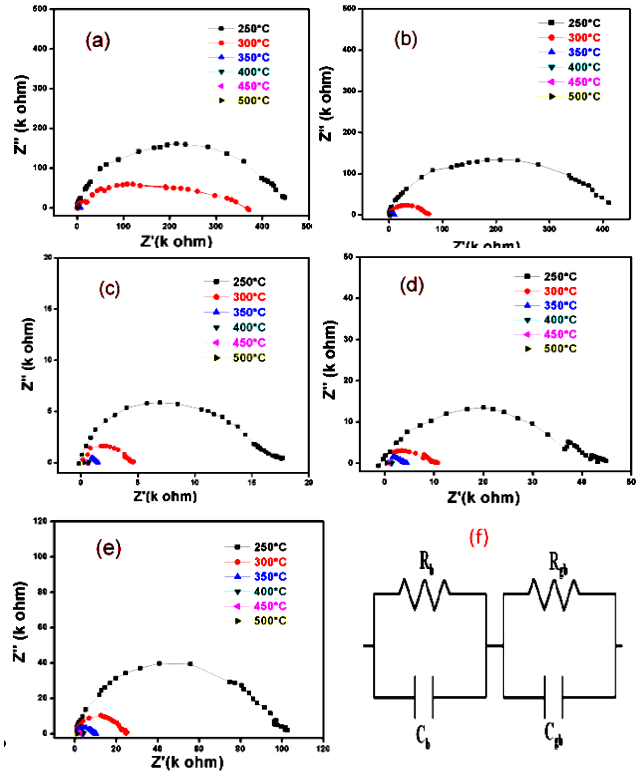

Fig. 9. Cole-Cole plots for (x) $Co_{0.5}Ni_{0.5}Fe_2O_4$ - (1−x) $Bi_{0.9}La_{0.1}FeO_3$ composites with (a) x = 0, (b) x = 0.25, (c) x = 0.40, (d) x = 0.55, (e) x = 1.0 and (f) equivalent circuit representation of grain and grain boundary contributions.

The values of resistance and capacitance corresponding to the bulk and grain boundary for temperature 250-500 ºC are given in **Table 4**, calculated by knowing the frequency for the peak maxima of semicircular arc and then using the relations:

$$\omega_{max} R_b C_b = 1 \quad (3)$$

$$\omega_{max} R_{gb} C_{gb} = 1 \quad (4)$$

The intercepts of these two semicircular arcs with the real axis (Z′) give us an estimate of the bulk resistance (R_b) in high frequency range and grain boundary resistance (R_{gb}) of the material in low frequency range.

It was observed that the slope of lines decrease towards Z′ axis with an increasing temperature. A well resolved semicircle is observed for each of the sample only at 250 °C. Similar type of cole–cole plots have been reported for $Sr_xBa_{1-x}Fe_{0.6}Sn_{0.4}O_{3-\varepsilon}$ ceramics [**52**]. It was observed that both resistance R_b and R_{gb} decreases with an increase in temperature, which shows the negative temperature coefficient of resistance (NTCR), correspond to a typical semiconducting property [**53, 54**]. The origin of semi conductivity in the grains may arise from a small but measurable oxygen loss during the synthesis process [**55**]. The electrical behavior can be represented in terms of equivalent circuit, which consists of series combination of

parallel RC circuit i.e. parallel combination of bulk resistance (R_b), bulk capacitance (C_b) and grain boundary resistance (R_{gb}), grain boundary capacitance (C_{gb}) respectively, is shown in **Fig. 9(f)**, which correspond to inter granular of material and grain boundary contribution, so they relax in different frequency region [**56**].

Table 4. Values of R_g, R_{gb} and C_b, C_{gb} for CNFO - BLFO composites for x = 0, 0.25, 0.40, 0.55 and 1.0.

Temperature °C		250 °C	300 °C	350 °C	400 °C	450 °C	500 °C
x = 0	R_b(kΩ)	450	290	6.5	1.85	0.775	0.375
	C_b (pF)	103.39	387.43	40.8	122.9	228.29	849.25
	R_{gb}(kΩ)	-----	375	7.35	2.05	0.880	0.400
	C_{gb} (pF)	-----	812.42	108.32	776	22618	19904
x = 0.25	R_b (kΩ)	410	72	8.75	2.65	1.050	0.492
	C_b (pF)	199.04	151.65	60.66	75.112	276	539.4
	R_{gb}(kΩ)	440	80	10.00	2.85	1.215	0.532
	C_{gb} (pF)	-----	631.88	79.61	279.36	163822	4988.6
x= 0.40	R_b (kΩ)	16.5	4.5	1.28	0.625	0.395	0.315
	C_b (pF)	165.87	144.75	138.22	283.08	403.12	16850
	R_{gb}(kΩ)	18	4.75	1.45	0.545	0.422	------
	C_{gb} (pF)	549.08	424.62	21.96	41739	1886.6	-----
x = 0.55	R_b (kΩ	43	8.5	3.55	1.250	0.780	0.425
	C_b (pF)	99.52	97.09	64.07	141.54	2564.1	53524
	R_{gb}(kΩ)	45	10	4.50	1.450	-------	------
	C_{gb} (pF))	227.47	203.62	1769.28	5490.8	-------	------
x = 1.00	R_b (kΩ	105	23.5	9.00	3.800	2.20	1.120
	C_b (pF)	159.23	127.38	58.97	83.80	103.39	555.79
	R_{gb}(kΩ)	-----	27.5	------	4.300	2.60	1.30
	C_{gb} (pF)	-----	379.13	------	740	874.92	20414.8

Conclusions

In summary, the magnetoelectric composites CNFO/BLFO consisting CNFO as the ferrite phase and BLFO as ferroelectric phase were successfully prepared by the solid state reaction method, where BLFO was prepared by sol-gel process and CNFO by solid state reaction method. The XRD pattern confirms the presence of constituent phases i.e. ferrite phase (CNFO) and ferroelectric phase (BLFO) of the composites. The average grain size as determined from FESEM micrographs is found to increase with the increase of CNFO content in the composites. Dielectric properties of the composites are improved with low value of dielectric loss. An anomaly in the dielectric constant around Neel temperature of BLFO suggests the magnetoelectric nature of the composites. The P-E hysteresis loops at room temperature indicates that there is presence of ferroelectric ordering and the coupling between ferroelectric and ferromagnetic orderings is confirmed through the magnetodielectric effect at room temperature. Impedance analysis in the composites provides evidence of space charge accumulation that vanishes at high frequency and high temperature and it also shows that the grain and grain boundary resistance decreases with rise in temperature which corresponds to the negative temperature coefficient of resistance (NTCR) behavior analogous to a semiconductor and suggests a Non-Debye type of electrical resistance. These observed values of dielectric constant and magnetization can be used for dynamic random access memories (DRAM) and in NTCR thermistors can be used for temperature sensors.

Acknowledgements

Authors would like to acknowledge the Council of Scientific and Industrial Research (CSIR), New Delhi, India for financial support under the grant 03 (1272)/13/EMR- II dated 12-04-2013 and 09/143(0801)/2011 EMR-I dated 2-11-2011.

Reference

1. Hill, Z.; Nicola A.; *J. Phys. Chem. B.*, **2000,** *104*, 6694. **DOI**: 10.1021/jp000114x
2. Hill, N.A.; *Annu. Rev. Mater. Res.*, **2002**, *32*, 1. **DOI**: 10.1146/annurev.matsci.32.101901.152309
3. Wang, Yao; Hu, Jiamian; Lin, Yuanhua; and Nan, Ce-Wen; *NPG Asia Mater*, **2010**, *2*, 2, 61. **DOI**:10.1038/asiamat.2010.32
4. Ryu J; Priya S; Uchino K; Kim HE; *J Electroceram.*, **2002**, *8*, 8107. **DOI**: 10.1023/A:1020599728432
5. Liu, Xian-Ming; Fu, Shao-Yun; Huang, Chuan-Jun; *Mater. Sci. Eng. B*, **2005**, *121*, 255. **DOI:**10.1016/j.mseb.2005.04.009
6. Singh, Hemant; Yadav, K.L.; *Journal of Alloys and Compounds*, **2014,** *585*, 805. **DOI:** 10.1016/j.jallcom.2013.09.20
7. Adhlakha, Nidhi; Yadav, K.L.; *J Mater Sci*., **2014,** *49*, 4423. **DOI:** 10.1007/s10853-014-8139-x
8. Kumar, Amit; Yadav, K. L.; Singh, Hemant; Pandu b, Ratnakar; Ravinder Reddy, P.; *Physica B* , **2010**, *405*, 2362. **DOI:** 10.1016/j.physb.2010.02.038
9. Kumar, Amit; Yadav, K.L.; *Physica B*, **2011**, *406*, 1763. **DOI:**10.1016/j.physb.2011.02.023
10. Singh, Hemant; Kumar, Amit; Yadav, K. L.; *Materials Science and Engineering B*, **2011** *176*, 540. **DOI:**10.1016/j.mseb.2011.01.010
11. Yang H; Wang H; He L; Shui L; Yao X; *J Appl Phys.*, **2010**, *108*, 074105. **DOI:** 10.1063/1.3490782
12. Babu SN; Hsu JH; Chen YS; Lin JG; *J Appl. Phys.*, **2010**, *107*, 09D919. **DOI:**10.1063/1.3360353
13. Chaix-Pluchery, O.; Cochard, C.; Jadhav, P.; Kreisel, J.; Dix, N.; Sánchez, F.; and Fontcuberta, J.; *Applied Physics Letters*, **2011**, *99*, 072901. **DOI:** 10.1063/1.3626595
14. M. Stratulat, Sergiu; Lu, Xiaoli; Morelli, Alessio; Hesse, Dietrich; Erfurth, Wilfried; and Alexe, Marin; *Nano Lett.*, **2013**, *13*, 3884. **DOI:** 10.1021/nl401965z
15. Comes, Ryan; Khokhlov, Mikhail; Liu, Hongxue; Lu, Jiwei; and Wolf, Stuart A.; *Journal Of Applied Physics*, **2012**, *111*, 07D914. **DOI:** 10.1063/1.3676413
16. Zhu, Yanyan; Cheng, Jinrong; Yu, Shengwen; Wu, Wenbiao; and Meng, Zhongyan; *Application of ferroelectrics, IEEE,* **2007**, *2007*, 415. **DOI:** 10.1109/ISAF.2007.4393283
17. Kumar, M; Yadav, K L.; *J Phys Chem Solids*, **2007,** *68*, 1791. **DOI:** 10.1016/j.jpcs.2007.05.006
18. Devan, RS; Kanamadi, CM; Lokare, SA; Chougule, BK; *Smart Mater Struct.*, **2006,** *15*, 1877. **DOI:** 10.1088/0964-1726/15/6/043
19. Lee, J-H.; Choi, H J.; Dongeun, Lee; Min G., Kim; Bark, C W.; Sangwoo, Ryu; Min-Ae, Oak; and Jang H M, *Phy. Rev. B.*, **2010**, *82*, 045113. **DOI:** 10.1103/PhysRevB.82.045113
20. Cheng, Z X; Li, A H; Wang, X L; Dou, S X; Ozawa, K; Kimura, H; Zhang, S J; and Shrout, T R; *J. Appl. Phys.*, **2008**, *103*, 07E507. **DOI:** 10.1063/1.2839325
21. Lee, D.; Kim, M. G.; Ryu, S.; Jang, H. M; and Lee, S. G; *Appl. Phys. Lett.*, **2005**, *86*, 222903. **DOI:** 10.1063/1.1941474
22. Kodama, T.; Kitayama, Y.; Tsuji, M.; Tamaura, Y.; *J. Appl. Phys.*, **1992**, *71*, 5926.
23. Vanidha, D.; Arunkumar A.; Rajagopan, S.; Kannan, R.; *J Supercond Nov Magn*., **2013**, *26*, 173. **DOI:** 10.1007/s10948-012-1705-z
24. Maqsood, A.; Khan, K.; *J. Alloys Compd*., **2011**, *509*, 3393. **DOI:**10.1016/j.jallcom.2010.12.082

25. Zhang, Jiaqi; Wang, Lei; Bian, Liang; Xu, Jinbao; Chang, Aiming; *Ceramics International*, **2014** *40*, 5173.
DOI: 10.1016/j.ceramint.2013.10.075
26. Buscaglia, M. T.; Buscaglia, V.; Viviani, M.; and Nanni, P.; *J. Am. Ceram. Soc*., **2001**, *84*, 2, 376.
DOI: 10.1111/j.1151-2916.2001.tb00665.x
27. Benguigui, L.; *Solid State Commun.*, **1972**, *11*, 825.
DOI: 10.1016/0038-1098(72)90280-3
28. Adhlakha, Nidhi; Yadav, K L; and Singh, Ripandeep; *Smart Mater. Struct.* **2014**, *23*, 105024.
DOI:10.1088/0964-1726/23/10/105024
29. P, Jayanta; and Krupanidhi, S. B.; *J. Appl. Phy.* **2008**, *104*, 024107.
DOI: 10.1063/1.2956695
30. Fawzi, A.S.; *Adv. Appl. Sci. Res.*, **2011,** *2*, 577.
31. Patankar, KK; Patil, SA; Sivakumar, KV; Mahajan, RP; Kolekar, YD; Kothale, MB; *Mater Chem Phys*, **2000**, *65*, 97.
DOI: 10.1016/S0254-0584(00)00216-9
32. Islam, RA; Priya, S; *J Mater Sci*, **2008,** *43*, 3560.
DOI: 10.1007/ s10853-008-2562-9
33. Gotardo, R A M; Viana, D S F; Olzon-Dionysio, M; Souza, S D; Garcia, D; Eiras, J A; Alves, M F S; Cotica, L F; Santos, I A; and Coelho, A A; *J. Appl. Phys.*, **2012,** *112*, 104112.
DOI:10.1063/1.4766450
34. Slonczewski, J. C; *J. Appl. Phys.* **1961**, 32, 253.
DOI:10.1063/1.2000425
35. Torres, T.E.; Roca, A.G.; Morales, M.P.; Ibarra, A.; Marquina, C.; Ibarra, M.R.; and Goya, G.F.; *Journal of Physics: Conference Series*, **2010**, *200*, 072101.
DOI:10.1088/1742-6596/200/7/072101
36. Kingery, W.D.; *Introduction to Ceramics*, **1960,** Wiley, New York.
37. Berkowitz, A. E.; Schuele, W. J.; *J. Appl. Phys.* **1959**, *30*, S134.
DOI: 10.1063/1.2185853
38. Zhang, Min; Zi, Zhenfa; Liu, Qiangchun; Zhang, Peng; Tang, Xianwu; Yang, Jie; Zhu, Xuebin; Sun, Yuping; and Dai, Jianming; *Advances in Materials Science and Engineering* **2013**, Article ID 609819.
DOI: 10.1155/2013/609819
39. Cullity, B.D.; Graham, C.D.; *Introduction to Magnetic Materials* Second Edition, IEEE Press.
40. Uestuener, K.; Katter, M.; and Rodewald, W.; *IEEE Ttransactions On Magnetics*, **2006,** *42*, 2897.
DOI: 10.1109/TMAG.2006.879889
41. Manjusha and Yadav, K.L.; *Advanced Materials Letters.*, **2014**, *5*, 11, 652.
DOI:10.5185/amlett.2014.4567
42. Palkar, VR; Kundaliya, DC; Malik, SK; Bhattacharya, S; *Phys Rev B.*,**2004**, *69*, 212102.
DOI: 10.1103/PhysRevB.69.212102
43. Patel, Piyush Kumar; Yadav, K.L.; *Physica B*, **2014**, *452*, 136.
DOI:10.1016/j.physb.2014.07.022
44. Katsufuji, T; and Takagi, H; *Phys. Rev. B*, **2001**, *64*, 054415.
DOI: 10.1103/PhysRevB.64.054415
45. Shen, Yajing; Sun, Junpeng; Li, Linglong; Yao, Yonggang; Zhou, Chao; Su, Ran; and Yang, Yaodong; *J. Mater. Chem. C*, **2014**, *2*, 2545.
DOI: 10.1039/C4TC00008K
46. Fina, I.; Dix, N.; Fàbrega, L.; Sánchez, F.; Fontcuberta, J.; *Thin Solid Films*, **2010,** *518*, 4634.
DOI:10.1016/j.tsf.2009.12.048
47. Palai, R.; Schmid, H.; Scott, J.F.; and Katiyar, *R.S.; Phys. Rev. B*, **2010**, *81*, 064110.
DOI: 10.1103/PhysRevB.81.139903
48. Islam, RA; Priya, S; *Adv Condes Matter Phys.*, **2012**, *2012*, 320612.
DOI:10.1155/2012/320612
49. Pahuja, P; Sharma, R; Prakash, C; and Tandon, R P; *Ceram. Int.*, **2013**, *39*, 9435.
DOI: 10.1016/j.ceramint.2013.05.061
50. Scott, J F; *J. Phys.: Condens. Matter*, **2008**, *20*, 021001.
DOI:10.1088/0953-8984/20/02/021001
51. Fan., J.; Sale, F. R.; *J. European Ceramic Society*, **2000**, *20*, 2743.
DOI: 10.1016/S0955-2219(00)00230-2
52. Yuan, C L; Liu, X Y; Jwxu; Wzhang, X; and Zhou, C R; *Bull. Mater. Sci.*, **2012**, *35*, 425.
DOI :10.1007/s12034-012-0294-6.
53. Kumari, K.; Prasad, K.; Yadav, K. L.; Sen, S.; *Brazilian J. Phys.*, **2009**, *39*, 297.
DOI: 10.1590/S0103-97332009000300010
54. Rawat, Meera; Yadav K. L., Kumar, Amit; Patel, Piyush Kumar; Adhlakha, Nidhi; Rani, Jyoti; *Adv. Mat. Lett.* **2012,** *3*, 286.
DOI: 10.5185/amlett.2012.2322
55. Kumar Patel, Piyush; Yadav, K. L.; and Kaur, Gurpreet; *RSC Adv.* **2014**, *4*, 28056.
DOI: 10.1039/C4RA03502J
56. Prasad, K.; Lily; Kumari, K.; Chandra, K.P.; Yadav, K.L.; Sen, S.; *Appl. Phys. A*., **2007,** *88*, 377.
DOI: 10.1007/s00339-007-3989-6

